Oxygen reduction electrocatalysts sophisticated by using Pt nanoparticle-dispersed ionic liquids with electropolymerizable additives

Oxygen reduction electrocatalysts sophisticated by using Pt nanoparticle-dispersed ionic liquids with electropolymerizable additives

Reiko Izumi,[a] Yu Yao,[a] Tetsuya Tsuda,*[a] Tsukasa Torimoto[b] and Susumu Kuwabata*[a]

[a]Department of Applied Chemistry, Graduate School of Engineering, Osaka University
2-1 Yamada-oka, Suita, Osaka 565-0871, Japan
*E-mail: kuwabata@chem.eng.osaka-u.ac.jp; ttsuda@chem.eng.osaka-u.ac.jp

[b]Department of Materials Chemistry, Graduate School of Engineering, Nagoya University
Furo-cho, Chikusa-ku, Nagoya, Aichi 464-8603, Japan

Abstract

The electropolymerization reaction of protic organic salt (POS) diphenylammonium hydrogen sulfate ($[DPA][HSO_4]$) in the solid state proceeds in a N_2-saturated 0.1 M $HClO_4$ aqueous solution, and conductive poly(diphenylamine) is formed without difficulty. This reaction has also been observed at the thin ionic liquid (IL) layer between Pt nanoparticles and carbon support on Pt nanoparticle-modified carbon electrocatalysts prepared using a *N,N*-diethyl-*N*-methylammonium hydrogen sulfate ($[DEMA][HSO_4]$) protic IL with a $[DPA][HSO_4]$ POS. Similar Pt nanoparticle electrocatalysts are fabricated using different electropolymerizable additives, including phenylammonium hydrogen sulfate ($[PhNH_3][HSO_4]$). A local electropolymerization reaction at the IL layer can confer a better electrochemical surface area and mass activity retention rates on oxygen reduction electrocatalysts. The performance of the resulting electrocatalysts is dependent on the electropolymerizable species.

1. Introduction

Polymer electrolyte fuel cells (PEFCs) are currently attracting much attention owing to their potential for use in clean energy generation systems for households and automobiles.[1-3] Their advantages include environmental friendliness, high power density, low operating temperatures, high start-up performance, and compactness. However, they also have several drawbacks that need to be overcome. One of the biggest problems is that PEFCs require expensive Pt-based electrocatalysts for enhancing the oxygen reduction reaction (ORR) at a cathode, as the ORR is considerably slower than the fuel oxidation reaction at an anode. Various approaches have been taken to reduce Pt usage and to improve catalytic activity, e.g., alloying Pt nanoparticles with low-cost transition metals,[4-6] crystallographic control of Pt nanoparticles,[4-6] utilization of ionic liquids (ILs) with high oxygen solubility,[7] and Pt surface modification by specific amine capping.[8] Another problem is catalyst degradation, which determines the fuel cell lifetime, especially under high-output-fluctuation operation, such as in automobile applications. It is generally considered that the catalyst is degraded by corrosion of the carbon support by Pt nanoparticles,[9-12] which induces Pt nanoparticle aggregation via Ostwald ripening. Several approaches for improving the durability of the Pt catalyst have been proposed, including the use of chemically inert supports, e.g., sp^2-carbon materials (carbon nanotubes[13] and graphene[14]), non-carbon materials,[15,16] and silica-coated carbon materials.[17] However, further novel approaches are expected to be developed in the future.

ILs are anhydrous liquid salts, with melting or eutectic points below room temperature, and are a subset of molten salts. Owing to their moderate ion-ion interactions and physicochemically stable ionic structures, they have interesting properties, such as negligible vapor pressure, relatively high ionic conductivity, a wide electrochemical window, good thermal stability, and antistatic properties. In previous work, we succeeded in preparing functional Pt nanoparticle-supported carbon electrocatalysts by agitating a mixture of carbon materials and Pt nanoparticle-dispersed ILs,[18-23] which were produced by magnetron sputtering onto the ILs

under reduced pressure.[24-26] The obtained electrocatalysts showed high durability that was attributed to the presence of a thin IL layer between the Pt nanoparticles and the carbon support, i.e., the IL layer suppressed corrosion of the carbon support.[22] Based on these findings, we then designed a unprecedented approach to create Pt nanoparticle-modified electrocatalysts with high catalytic activity and superior durability using a *N*,*N*-diethyl-*N*-methylammonium hydrogen sulfate ([DEMA][HSO$_4$], **1**) protic IL (PIL) with a polymerizable diphenylammonium hydrogen sulfate ([DPA][HSO$_4$]) protic organic salt (POS).[23] The obtained Pt nanoparticle-supported carbon catalysts showed anomalous catalytic behavior; that is, the durability was enhanced and the mass activity was increased during the potential cycling durability test, despite the decrease in the electrochemical surface area (ECSA) of the catalyst. These unexpected results could potentially be ascribed to the formation of a conductive polymer, poly(diphenylamine), by the electrochemical oxidation of [DPA][HSO$_4$] at the IL layer between Pt nanoparticles and the carbon support during the durability test. However, further evidence was required to fully elucidate the process. In the present study, we examined the electropolymerization process on the Pt nanoparticle-supported carbon catalysts prepared in a PIL **1** and [DPA][HSO$_4$] POS mixture to establish a novel approach for designing high-performance electrocatalysts. Based on the results, several Pt nanoparticle-supported carbon electrodes were prepared using different types of electropolymerizable additives, and the influence of the additives on catalytic performance was investigated.

2. Experimental Section

2.1 Chemicals

N,*N*-diethyl-*N*-methylamine (99%), diphenylamine (98.5%), and 3-methylthiophene (98%, 3MT) were purchased from Tokyo Chemical Industry Co., Ltd. Sulfuric acid (95%), 3,4-ethylenedioxythiophene (97%, EDOT), and potassium bromide (KBr) were products of Wako Pure Chemicals Co., Ltd. Phenylamine (95%) and pyrrole (98%) were obtained from Sigma

Aldrich. PIL ([DEMA][HSO₄], **1**) and POSs ([DPA][HSO₄], phenylammonium hydrogen sulfate ([PhNH₃][HSO₄])) were synthesized by simple stoichiometric neutralization of respective amines with sulfuric acid in organic or aqueous solutions and subsequent solvent removal under vacuum.[27,28] *N,N,N*-trimethyl-*N*-propylammonium bis(trifluoromethanesulfonyl)amide ([N$_{1,1,1,3}$][Tf$_2$N], **2**) was purchased from Kanto Chemical Co., Inc. IL **2** was purified prior to use as described elsewhere.[22]

2.2 Electropolymerization test of a [DPA][HSO₄]-coated ITO electrode

A small amount of [DPA][HSO₄] salt powder was placed on a pre-cleaned indium tin oxide (ITO) substrate (1 × 3 cm) heated on a hotplate. When the salt was melted at around 373 K, it was spread over the substrate with a spatula, followed by heating at 373 K for 30 min. The silver paste was put on top of the substrate to make good electrical contact. A silver/silver chloride (Ag/AgCl) and a Pt foil were used as reference and counter electrodes, respectively. Electropolymerization testing was performed in 0.1 M HClO₄ under two potential cycling conditions used for the evaluation of catalytic activity. One was an electrochemical cleaning process (100 cycles at a sweep rate of 50 mV s⁻¹ between 0.05–1.15 V), and the other was a durability test (15,000 cycles at a sweep rate of 500 mV s⁻¹ between 1.0–1.5 V). The [DPA][HSO₄] subjected to the electropolymerization test was carefully removed from the ITO electrode and was washed with ethanol before analysis of its morphology observation by scanning electron microscopy (SEM) and chemical structure by Fourier transform infrared (FTIR) spectroscopy.

2.3 Preparation of Pt nanoparticle-supported carbon catalysts

As previously reported,[22,23] sputter deposition of Pt with a direct current mode onto 0.4 mL of IL **1** (2.7 mmol) at room temperature (298 ± 2 K) was conducted at a sputter current of 40 mA for 30 min in a Cressington 108 Auto/SE sputter coater under dry Ar (99.999%), the pressure

of which did not exceed 7 ± 1 Pa. Carbon black (1.5 mg, Cabot, Vulcan®-XC72) and [DPA][HSO$_4$] (1.2 g, 4.5 mmol) were added to the obtained Pt-sputtered [DEMA][HSO$_4$] (0.4 mL, Pt concentration: 0.31 wt%) in a vial, and it was stirred at 373 K for 20 min. Finally, the homogenized mixture was agitated at 473 K for 2 h, washed with ultrapure water and ethanol, and then dried *in vacuo* for 15 h to obtain the desired catalyst, Pt/[DPA][HSO$_4$]·**1**/C.[22,23] For the preparation of catalyst, several electropolymerizable additives and two types of ILs were used. The [DPA][HSO$_4$]-free catalyst, Pt/−·**1**/C, was similarly prepared without addition of [DPA][HSO$_4$] as described in our previous paper.[23] Other Pt nanoparticle-supported carbon catalysts, Pt/[PhNH$_3$][HSO$_4$]·**1**/C, Pt/3MT·**1**/C, Pt/pyrrole·**1**/C, and Pt/EDOT·**1**/C were prepared by a similar procedure but with 1.2 g (6.3 mmol) of [PhNH$_3$][HSO$_4$], 22 mg (0.22 mmol) of 3MT, 34 mg (0.51 mmol) of pyrrole, and 71 mg (0.50 mmol) of EDOT, respectively, as electropolymerizable additives instead of [DPA][HSO$_4$]. For preparation of the catalysts with 3MT, pyrrole, and EDOT, the heating temperature was set at 353 K, which is lower than the boiling point of the charge-neutral additives. Pt/diphenylamine·**2**/C was prepared in a similar way by agitating a mixture of Pt-sputtered IL **2** (0.4 mL, 1.5mmol) and diphenylamine (125 mg, 0.739 mmol) as electropolymerizable additives and Vulcan® at 573 K for 2 h, followed by washing several times with acetonitrile. Additive-free Pt/−·**2**/C was prepared as described in previous papers.[22,23] A commercially available Pt nanoparticle catalyst (TEC10V30E, Tanaka Kikinzoku Kogyo) was used as a reference.

2.4 Characterization

The electrochemically treated [DPA][HSO$_4$] was rinsed with ethanol several times. The morphology of the [DPA][HSO$_4$] sample was examined using a Hitachi S-3400N SEM under an accelerating voltage of 10 kV. The sample (0.2 mg), which was previously uniformly mixed in a mortar with well-dried KBr (40 mg), was pressed to obtain a translucent pellet for FTIR spectroscopy. FTIR spectroscopy was conducted on a Perkin Elmer Spectrum 100 instrument

in a wavelength range of 400–4000 cm^{-1}. The morphology of the electrocatalysts was observed by Transmission electron microscopy (TEM) (Hitachi H-7650) at an acceleration voltage of 100 kV. Pt concentration in the Pt-sputtered [DEMA][HSO$_4$] and Pt loading amount in the resulting electrocatalysts were determined by subjecting the solutions obtained by dissolving Pt nanoparticles in hot aqua regia to inductively coupled plasma atomic emission spectrometry (ICP-AES; Shimadzu ICPS-7510).

2.5 Electrochemical measurements

Electrocatalytic activities were examined by a computer-controlled Hokuto Denko HZ-7000 potentiostat/galvanostat. The electrochemical measurements were conducted using a three-electrode cell at ca. 298 K with a glassy carbon (GC) rotating disk electrode (surface area = 0.196 cm^2). A Pt mesh, a Ag/AgCl/KCl saturated aqueous solution double-junction electrode, and a 0.1 M HClO$_4$ aqueous solution were used as the counter electrode, the reference electrode, and the electrolyte, respectively. The catalyst ink was prepared by ultrasonically dispersing the Pt catalyst (1.48 mg) in 2-propanol (1.0 mL) for 5 min. A 10 μL volume of the ink was uniformly spread onto the GC disk electrode and dried in air. Subsequently, to fix the catalyst on the GC disk surface, the electrode was covered with Nafion® solution (10 μL, 0.1 wt% diluted with 2-propanol), and the produced working electrode was set in an electrode rotator (AFMSRCE, Pine Instruments). All potential values were referenced to the reversible hydrogen electrode (RHE). Prior to measurements, the working electrode was electrochemically cleaned by 40–100 potential sweeps between 0.05 and 1.2 V at a scan rate of 50 mV s^{-1} under a N$_2$ atmosphere until the cyclic voltammograms were stabilized. The ECSA of Pt nanoparticles was determined based on the passed charge for hydrogen adsorption or desorption estimated from the obtained voltammogram after subtracting the double-layer charge currents:

$$\text{ECSA} = \frac{Q_\text{H} \times 10^2}{210 \times M_\text{Pt}} \qquad (1)$$

where Q_H (µC) is the amount of charge during hydrogen adsorption/desorption[29] and M_{Pt} (µg) is the mass of Pt on the GC working electrode. For comparison, the average amount of charge associated with the formation of a hydrogen adsorption/desorption monolayer on smooth polycrystalline Pt is 210 µC cm^{-2}. Catalyst durability was estimated by the standard degradation test recommended by the Fuel Cell Commercialization Conference of Japan (FCCJ).[30,31] In this test, the cathode of a proton-exchange membrane fuel cell is overloaded by applying the potential cycling between 1.00 and 1.50 V at 500 mV s^{-1} to enhance carbon corrosion, allowing catalyst durability to be electrochemically evaluated in a short time period. To obtain additional insights into catalyst deterioration, ECSA retention was estimated as follows:

$$\text{Surface retention rate (\%)} = \frac{\text{ECSA estimated at each cycle (m}^2\text{ g}^{-1})}{\text{initial ECSA (m}^2\text{ g}^{-1})} \qquad (2)$$

The ORR was performed in an O$_2$-saturated 0.1 M HClO$_4$ aqueous solution and characterized by rotating disk electrode linear sweep voltammetry (RDE-LSV) in the anodic potential sweep at 10 mV s^{-1} and five different rotation speeds (200, 400, 800, 1200, and 1600 rpm). The obtained cathodic current due to ORR is described by the Koutecký-Levich equation:

$$\frac{1}{I} = \frac{1}{I_k} + \frac{1}{B\,\omega^{1/2}} \qquad (3)$$

where $B = 0.62nFAC^*D^{2/3}v^{-1/6}\omega^{1/2}$. In the above expression, I is the experimentally measured current at 0.85 V, I_k is the kinetic current, $\omega^{1/2}$ is the electrode rotation rate, n is the electron transfer number, F is the Faraday constant, A is the electrode surface area, C^* is the O$_2$ concentration in the electrolyte, D is the diffusion coefficient of O$_2$ in the electrolyte, and v is the viscosity of the electrolyte. Based on this, I_k was estimated from the intercept of the Koutecký-Levich plot (I^{-1} *vs.* $\omega^{-1/2}$) and normalized with respect to the Pt loading of each catalyst to obtain mass activities, with mass activity retentions determined according to eqn (4):

$$\text{Catalytic activity retention rate } (\%) = \frac{\text{mass activity estimated after 15,000 cycles (A g}^{-1})}{\text{initial mass activity (A g}^{-1})} \quad (4)$$

3. Results and discussion

In order to explain the anomalous behavior of the Pt nanoparticle-supported carbon catalysts prepared in a PIL **1** and [DPA][HSO$_4$] POS mixture during the durability test,[23] electrochemical examination of the [DPA][HSO$_4$]-coated transparent ITO electrode was conducted in a N$_2$-saturated 0.1 M HClO$_4$ aqueous solution. The electrode and cell used are depicted in Fig. 1a and 1b. Notably, the [DPA][HSO$_4$] salt was firmly deposited on the ITO electrode surface without dissolution in the electrolyte solution, even when the electrochemical measurement was initiated. The electrochemical measurement was conducted under two different potential cycling conditions: first, the condition for electrochemical cleaning (0.05–1.15 V *vs*. RHE, 50 mV s^{-1}, 100 cycles); and second, the condition for the durability test (1.0–1.5 V, 500 mV s^{-1}, 15,000 cycles). Soon after immersing the [DPA][HSO$_4$]-coated ITO into the aqueous solution, as shown in Fig. 1b, the transparent [DPA][HSO$_4$] layer changed to a white color, indicating formation of diphenylamine by the deprotonation of the [DPA]$^+$ (pK_a = 0.78).[32] Fig. 1c shows typical cyclic voltammograms recorded at the [DPA][HSO$_4$]-coated ITO electrode under the electrochemical cleaning condition. At the first cycle, only an oxidation wave was observed at around 1.10 V. With increasing cycling number, the oxidation peak at 1.10 V became smaller, while a broad redox wave at around 0.4–0.9 V appeared and gradually increased. The white [DPA][HSO$_4$] layer varied to green from its edge immediately after the potential cycling was started (Fig. 1d). This green-colored area increased upon cycling. The resulting green [DPA][HSO$_4$] film reversibly changed color from dark-green to yellow-green during the potential cycling. A video clip of this electrochromic behavior can be seen in Movie S1. These electrochemical and electrochromic behaviors are consistent with previous reports on the electropolymerization of diphenylamine to poly(diphenylamine).[33-36] Similar behavior was also recognized under the conditions of the durability test. SEM images of the electrochemically

8

treated [DPA][HSO$_4$] were very much like ones reported previously (Fig. S1†).[36] Further

investigation of the [DPA][HSO$_4$]-coated ITO before and after the potential cycling tests was

conducted by FTIR spectroscopy. Fig. 2 shows the FTIR spectra of diphenylamine, as-

synthesized [DPA][HSO$_4$], and [DPA][HSO$_4$] after the two potential cycling tests. The strong

band at ca. 815 cm^{-1}, which is assigned to *para*-coupled monomeric unit for

poly(diphenylamine), appeared only at the [DPA][HSO$_4$] after the cycling tests,[33-36] confirming

that the conductive poly(diphenylamine) was formed from [DPA][HSO$_4$] layer deposited on

the ITO electrode in the 0.1 M HClO$_4$ aqueous solution.

Cyclic voltammetry was carried out in aqueous solution to clarify whether the

electropolymerization of [DPA][HSO$_4$] occurs by potential cycling even in the actual Pt

nanoparticle-supported carbon catalyst prepared using [DPA][HSO$_4$] and in Pt nanoparticle-

monodispersed PIL **1** (Pt/[DPA][HSO$_4$]·**1**/C). Fig. 3a shows the voltammograms obtained

during electrochemical cleaning of Pt/[DPA][HSO$_4$]·**1**/C. A large oxidation current at 0.90–

1.15 V was observed in the first cycle, and clear redox waves appeared at 0.70–0.80 V after the

second cycle (up to the tenth cycle). This behavior is essentially consistent with that of

[DPA][HSO$_4$]-coated ITO (Fig. 1c), indicating that poly(diphenylamine) was indeed formed in

Pt/[DPA][HSO$_4$]·**1**/C during the electrochemical cleaning. The redox waves derived from

poly(diphenylamine) formation and oxidation/reduction of the Pt surface appeared smaller and

larger, respectively, after further cycling. This electrode behavior was not observed in the

electrocatalyst prepared with only PIL **1** (Pt/−·**1**/C) (Fig. 3b). Thus, we concluded that the high

catalytic activity and durability of Pt/[DPA][HSO$_4$]·**1**/C were due to the formation of

poly(diphenylamine) by the electropolymerization of [DPA][HSO$_4$].

The aforementioned electrocatalyst fabrication process was applied to other ILs and

electropolymerizable additive mixtures to understand their influence on catalytic performance.

[PhNH$_3$][HSO$_4$], 3MT, pyrrole, and EDOT were used as the electropolymerizable additives for

PIL **1** instead of [DPA][HSO$_4$] to synthesize the electrocatalysts Pt/[PhNH$_3$][HSO$_4$]·**1**/C,

Pt/3MT·**1**/C, Pt/pyrrole·**1**/C, and Pt/EDOT·**1**/C, respectively. However, the solubility of 3MT in **1** was very low. In addition to those mixtures, $[N_{1,1,1,3}][Tf_2N]$, IL **2**, with diphenylamine as an electropolymerizable additive was employed for fabrication of Pt/diphenylamine·**2**/C. TEM images of the five new electrocatalysts are shown in Fig. 4. For comparison, TEM images of the previously reported Pt nanoparticle-supported carbon catalysts, prepared under the similar conditions,[23] Pt/[DPA][HSO$_4$]·**1**/C, Pt/–·**1**/C, Pt/–·**2**/C, and TEC10V30E are also shown. For Pt/[PhNH$_3$]·**1**/C, Pt/3MT·**1**/C, and Pt/diphenylamine·**2**/C, the Pt nanoparticles were homogeneously dispersed on the carbon support. Their Pt nanoparticle size distributions were analyzed; the results are shown in Fig. S2† and Table 1, along with those for the comparative catalysts. The mean particle size of Pt nanoparticles for Pt/[PhNH$_3$][HSO$_4$]·**1**/C, Pt/3MT·**1**/C, and Pt/diphenylamine·**2**/C was 2.6–3.4 nm, and the Pt loading amount was ~20–21 wt%. These values were nearly equivalent to those for the comparative catalysts (Table 1). By contrast, the morphologies of the Pt/pyrrole·**1**/C and Pt/EDOT·**1**/C clearly differed from those of other catalysts, as thermopolymerization and/or thermal decomposition of the pyrrole and EDOT readily proceeded in [DEMA][HSO$_4$] during the heating step in the electrocatalyst preparation process. For this reason, Pt/pyrrole·**1**/C and Pt/EDOT·**1**/C showed no catalytic activity. Therefore, detailed electrochemical experiments were carried out using the other three catalysts, Pt/[PhNH$_3$][HSO$_4$]·**1**/C, Pt/3MT·**1**/C, and Pt/diphenylamine·**2**/C. Fig. S3† indicates the cyclic voltammograms recorded for the three catalysts in a N$_2$-saturated 0.1 M HClO$_4$ aqueous solution during electrochemical cleaning. As a comparison, results for the Pt/–·**2**/C are also given. The voltammogram recorded for Pt/–·**2**/C showed only growth of waves related to Pt, whereas the appearance and growth of other redox waves were seen at 0.5–0.9 V in other voltammograms, suggesting electrochemical polymerization of the additives proceed in the catalyst layers. The growth of redox waves was smallest in the voltammogram of Pt/3MT·**1**/C, probably owing to the low solubility of 3MT in [DEMA][HSO$_4$].

10

Cyclic voltammograms obtained for Pt/[PhNH$_3$][HSO$_4$]·**1**/C, Pt/3MT·**1**/C, Pt/diphenylamine·**2**/C, and Pt/[DPA][HSO$_4$]·**1**/C in a N$_2$-saturated 0.1 M HClO$_4$ before and after the durability test (15,000 cycles), simulating actual fuel cell operation, are shown in Fig. 5. Those for Pt/−·**1**/C, Pt/−·**2**/C, and TEC10V30E are given in Fig. S4† for reference. In all the voltammograms, hydrogen adsorption/desorption and platinum oxidation/reduction redox waves were observed at 0.10–0.35 and 0.80–1.20 V, respectively. The ECSAs estimated from charges consumed by hydrogen desorption in the voltammograms before the durability test are given in Table 1. Pt/[PhNH$_3$][HSO$_4$]·**1**/C, Pt/3MT·**1**/C, Pt/diphenylamine·**2**/C, and Pt/[DPA][HSO$_4$]·**1**/C showed initial ECSAs of 40–42 m^2 g^{-1}, similar to the values obtained for the electropolymerizable additive-free Pt/−·**1**/C and Pt/−·**2**/C, but slightly smaller than that of TEC10V30E, probably owing to a trace of the residual IL on the Pt nanoparticles meagerly preventing the adsorption of H atoms.[37,38] Fig. 6 shows the variation in the ECSA and the surface retention rate for the ECSA on the catalysts shown in Table 1, as a function of potential cycling number, which provides important insights into the durability of the catalysts. ECSAs of all the catalysts prepared in this study increased during the first several thousand cycles, because the residual IL was removed from catalysts,[22,23] and gradually decreased thereafter. High surface retention rates for ECSAs (over 73%) were obtained at 15,000 cycles, although that of TEC10V30E was almost 30%. Interestingly, the ECSA retention rate for Pt/[DPA][HSO$_4$]·**1**/C was nearly 100%, even after 15,000 cycles. During the durability test, carbon corrosion usually proceeds via the oxidation of functional groups on the carbon support,[9-12] but it is inhibited by the existence of a thin IL layer between the Pt nanoparticles and the carbon support.[22,23] Adding the electropolymerizable additives, especially [PhNH$_3$][HSO$_4$] and [DPA][HSO$_4$], to the ILs seems to be an effective approach for further improvement. As depicted in Fig. S5†, after the durability test, a large number of Pt nanoparticles aggregated but did not detach from the carbon support, compared with

TEC10V30E, which was deteriorated by carbon corrosion, causing the detachment of Pt nanoparticles.[39] This is in agreement with the trend of surface retention rates for the ECSA.

The ORR performances before and after the durability test were examined by RDE-LSV (Fig. 7 and S6†). The half-wave potential differences ($\Delta E_{1/2}$) estimated from the obtained RDE-LSV curves are shown in these figures. Interestingly, the $E_{1/2}$ values of the catalysts with electropolymerizable additives were positively shifted after the durability test, indicating that the catalytic activities were enhanced during the test. The mass activities before and after the durability test for all catalysts are displayed, together with their catalytic activity retention rate for the mass activity, in Fig. 8 and Table 1. All the electrocatalysts with electropolymerizable additives showed retention rates over 100%, but rates for other electrocatalysts were unable to exceed even 90%; for example, that of TEC10V30E was as small as 63%. These results strongly suggest that the formation of a conductive polymer derived from electropolymerizable additives at the IL layer between Pt nanoparticles and the carbon support contributes to the enhancement of mass activity after the durability test, as well as the favorable surface retention rate estimated from the ECSA data.

4. Conclusion

We revealed that poly(diphenylamine) is formed by electropolymerization during the potential cycling of the [DPA][HSO$_4$]-coated ITO electrode in a N$_2$-saturated 0.1 M HClO$_4$ aqueous solution. Similar behavior was also observed in the case of the Pt/[DPA][HSO$_4$]·**1**/C electrocatalyst, suggesting that the increase in mass activity observed at the electrocatalyst after the durability test was due to the formation of conductive poly(diphenylamine) at the IL layer between the Pt nanoparticles and the carbon support. Similarly, addition of other electropolymerizable additives, [PhNH$_3$][HSO$_4$], 3MT, and diphenylamine, to the Pt nanoparticle-dispersed ILs enhanced the catalytic performance. This finding has important implications for designing novel functional ORR electrocatalysts. Further improvement of the

electrocatalysts prepared by the approach established in this article will be achieved through more elaborate selection of electropolymerizable additives.

Conflicts of interest

There are no conflicts to declare.

Footnotes

† Electronic supplementary information (ESI) available: Additional data (Fig. S1–S6 and Movie S1) and captions for Movies S1. See DOI:10.1039/((please add manuscript number))

Received: ((will be filled in by the editorial staff))
Revised: ((will be filled in by the editorial staff))
Published online: ((will be filled in by the editorial staff))

References

1. V. Mehta, J. S. Cooper, *J. Power Sources*, 2003, **114**, 32–53.

2   Y. Wang, K. S. Chen, J. Mishler, S. C. Cho, X. C. Adroher, *Applied Energy*, 2011, **88**, 981–1107.

3   M. K. Debe, *Nature*, 2012, **486**, 43–51.

4   C. Chen, Y. Kang, Z. Huo, Z. Zhu, W. Huang, H. L. Xin, J. D. Snyder, D. Li, J. A. Herron, M. Mavrikakis, M. Chi, K. L. More, Y. Li, N. M. Markovic, G.A. Somorjai, P. Yang, V. R. Stamenkovic, *Science*, 2014, **343**, 1339–1343.

5   L. Zhang, L. T. Roling, X. Wang, M. Vara, M. Chi, J. Liu, S.-I. Choi, J. Park, J. A. Herron, Z. Xie, M. Mavrikakis, Y. Xia, *Science*, 2015, **349**, 412–416.

6   X. Zhao, S. Chen, Z. Fang, J. Ding, W. Sang, Y. Wang, J. Zhao, Z. Peng, J. Zeng, *J. Am. Chem. Soc.*, 2015, **137**, 2804–2807.

7   J. Snyder, T. Fujita, M. W. Chen, J. Erlebacher, *Nat. Mater.*, 2010, **9**, 904–907.

8   K. Miyabayashi, H. Nishihara, M. Miyake, *Langmuir*, 2014, **30**, 2936–2942.

9   R. Borup, J. Meyers, B. Pivovar, Y. S. Kim, R. Mukundan, N. Garland, D. Myers, M. Wilson, F. Garzon, D. Wood, P. Zelenay, K. More, K. Stroh, T. Zawodzinski, J. Boncella, J. E. McGrath, M. Inaba, K. Miyatake, M. Hori, K. Ota, Z. Ogumi, S. Miyata, A. Nishikata, Z. Siroma, Y. Uchimoto, K. Yasuda, K. Kimijima, N. Iwashita, *Chem. Rev.*, 2007, **107**, 3904–3951.

10 Y. Shao, G. Yin and Y. Gao, *J. Power Sources*, 2007, **171**, 558–566.

11 T. Ioroi, T. Akita, M. Asahi, S. Yamazaki, Z. Siroma, N. Fujiwara and K. Yasuda, *J. Power Sources*, 2013, **223**, 183–189.

12 A. P. Young, V. Colbow, D. Harvey, E. Rogers and S. Wessel, *J. Electrochem. Soc.*, 2013, **160**, F381–F388.

13 M. R. Berber, T. Fujigaya, K. Sasaki, N. Nakashima, *Sci. Rep.*, 2013, **3**, 1764.

14 D. Higgins, P. Zamani, A. Yu, Z. Chen, *Energy Environ. Sci.*, 2016, **9**, 357–390.

15 Y. J. Wang, D. P. Wilkinson, J. Zhang, *Chem. Rev.*, 2011, **111**, 7625–7651.

16 Y. Liu, W. E. Mustain, *J. Am. Chem. Soc.*, 2013, **135**, 530–533.

17 S. Takenaka, H. Miyamoto, Y. Utsunomiya, H. Matsune, M. Kishida, *J. Phys. Chem. C*, 2013, **118**, 774–783.

18 T. Tsuda, T. Kurihara, Y. Hoshino, T. Kiyama, K. Okazaki, T. Torimoto, S. Kuwabata, *Electrochemistry*, 2009, **77**, 693–695.

19 T. Tsuda, K. Yoshii, T. Torimoto, S. Kuwabata, *J. Power Sources*, 2010, **195**, 5980–5985.

20 K. Yoshii, T. Tsuda, T. Arimura, A. Imanishi, T. Torimoto, S. Kuwabata, *RSC Adv.*, 2012, **2**, 8262–8264.

21 M. Hirano, K. Enokida, K. Okazaki, S. Kuwabata, H. Yoshida, T. Torimoto, *Phys. Chem. Chem. Phys.*, 2013, **15**, 7286–7294.

22 K. Yoshii, K. Yamaji, T. Tsuda, H. Matsumoto, T. Sato, R. Izumi, T. Torimoto, S. Kuwabata, *J. Mater. Chem.*, *A* 2016, **4**, 12152–12157.

23 R. Izumi, Y. Yu, T. Tsuda, T. Torimoto, S. Kuwabata, *Adv. Mater. Interfaces*, 2018, **5**, 1701123.

24 T. Torimoto, K. Okazaki, T. Kiyama, K. Hirahara, N. Tanaka, S. Kuwabata, *Appl. Phys. Lett.*, 2006, **89**, 243117.

25 H. Wender, P. Migowski, A. F. Feil, S. R. Teixeira, J. Dupont, *Coord. Chem. Rev.*, 2013, **257**, 2468–2483.

26 L. Calabria, J. A. Fernandes, P. Migowski, F. Bernardi, D. L. Baptista, R. Leal, T. Grehl, J. Dupon, *Nanoscale*, 2017, **9**, 18753–18758.

27 S. Zang, M. S. Miran, A. Ikoma, K. Dokko, M. Watanabe, *J. Am. Chem. Soc*., 2014, **136**, 1690–1695.

28 S. Zang, K. Dokko, M. Watanabe, *Chem. Mater*., 2014, **26**, 2915–2926.

29 K. Yamamoto, D. M. Kolb, R. Kötz, G. Lehmpfuhl, *J. Electroanal. Chem. Interfacial Electrochem.*, 1979, **96**, 233–239.

30 Fuel Cell Commercialization Conference of Japan (FCCJ), Proposals of the development targets, research and development challenges and evaluations methods concerning PEFCs, URL: http://www.fccj.jp/pdf/23_01_kt.pdf

31 A. Iiyama, K. Shinohara, S. Iguchi, A. Daimaru, *Handbook of Fuel Cells – Fundamentals, Technology, and Application*, John Wiley & Sons, West Sussex, UK, 2009.

32 D. Dolman, R. Stewart, *Can. J. Chem.*, 1967, **45**, 903–910.

33 N. Comisso, S. Daolio, G. Mengoli, R. Salmaso, S. Zecchin, G. Zotti, *J. Electroanal. Chem. Interfacial Electrochem.*, 1988, **255**, 97–110.

34 A. Bagheri, M. E. Nateghi, A. Massoumi, *Synth. Met.*, 1998, **97**, 85–89.

35 C.-Y. Chung, T.-C. Wen, A. Gopalan, *Elecrochim. Acta*, 2001, **47**, 423–431.

36 U. Hayat, P. Bartlett, G. H. Dodd, *J. Electroanal. Chem.*, 1987, **220**, 287–294.

37 M. Sobota, M. Happel, M. Amende, N. Paape, P. Wasserscheid, M. Laurin, J. Libuda, *Adv. Mater.*, 2011, **23**, 2617–2621.

38 J. Arras, E. Paki, C. Roth, J. Radnik, M. Lucas, P. Claus, *J. Phys. Chem. C*, 2010, **114**, 10520–10526.

39 X. Zhao, A. Hayashi, Z. Noda, K. Kimijima, I. Yagi, K. Sasaki, *Electrochim. Acta*, 2013, **97**, 33–41.
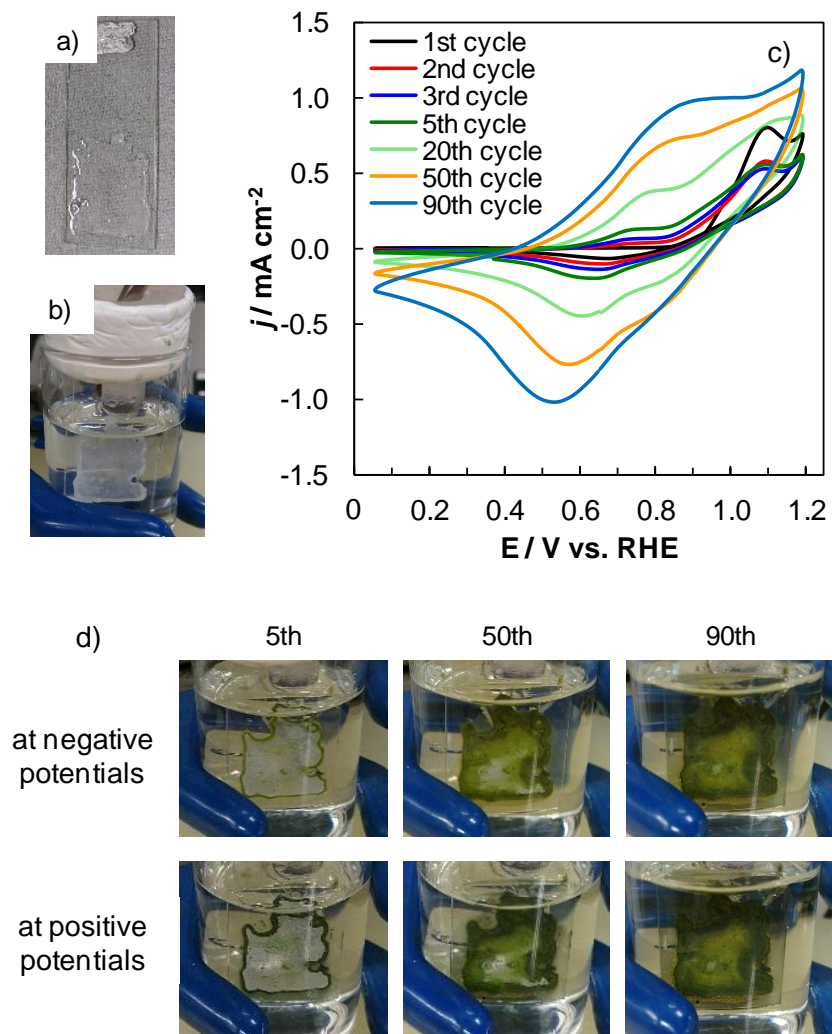
Fig. 1 Photo images of (a) a [DPA][HSO$_4$]-coated ITO electrode and (b) an electrochemical cell for the electropolymerization test. (c) Cyclic voltammograms recorded at a [DPA][HSO$_4$]-coated ITO electrode in a N$_2$-saturated 0.1 M HClO$_4$ aqueous solution during the electropolymerization test. (d) Photographs of the [DPA][HSO$_4$]-coated ITO electrode at each cycle number during the electropolymerization test.
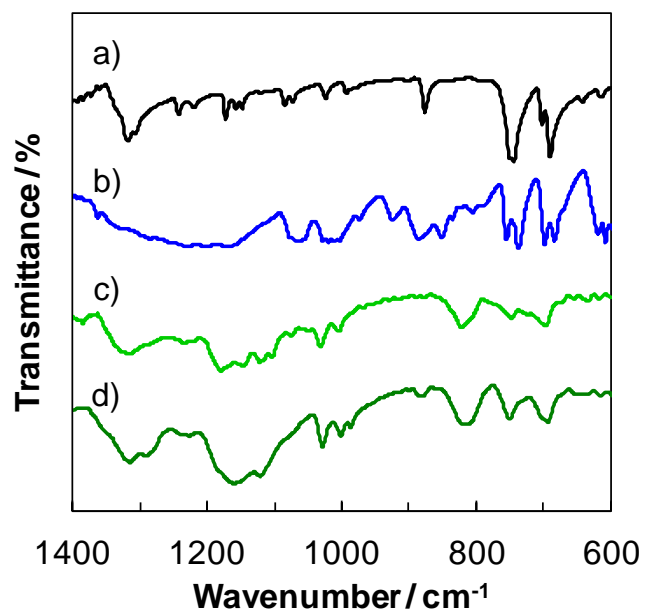
Fig. 2 FTIR spectra of (a) diphenylamine, (b) as-prepared [DPA][HSO$_4$], and specimen b after potential cycling by (c) electrochemical cleaning and (d) durability test (15,000 cycles).
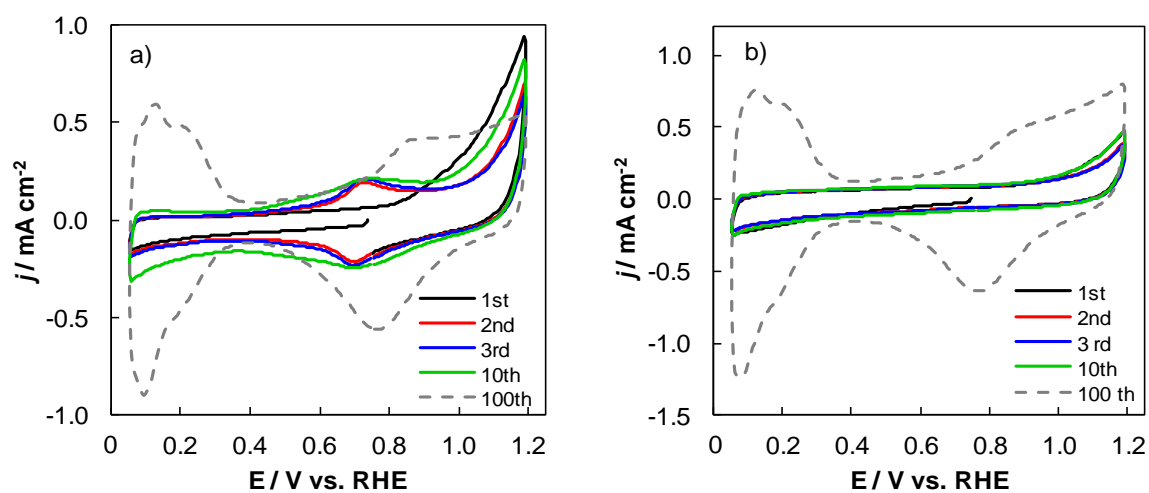
Fig. 3 Cyclic voltammograms recorded in a N_2-saturated 0.1 M $HClO_4$ aqueous solution at a scan rate of 50 mV s^{-1} during the electrochemical cleaning of (a) Pt/[DPA][HSO$_4$] ·**1**/C and (b) Pt/–·**1**/C.
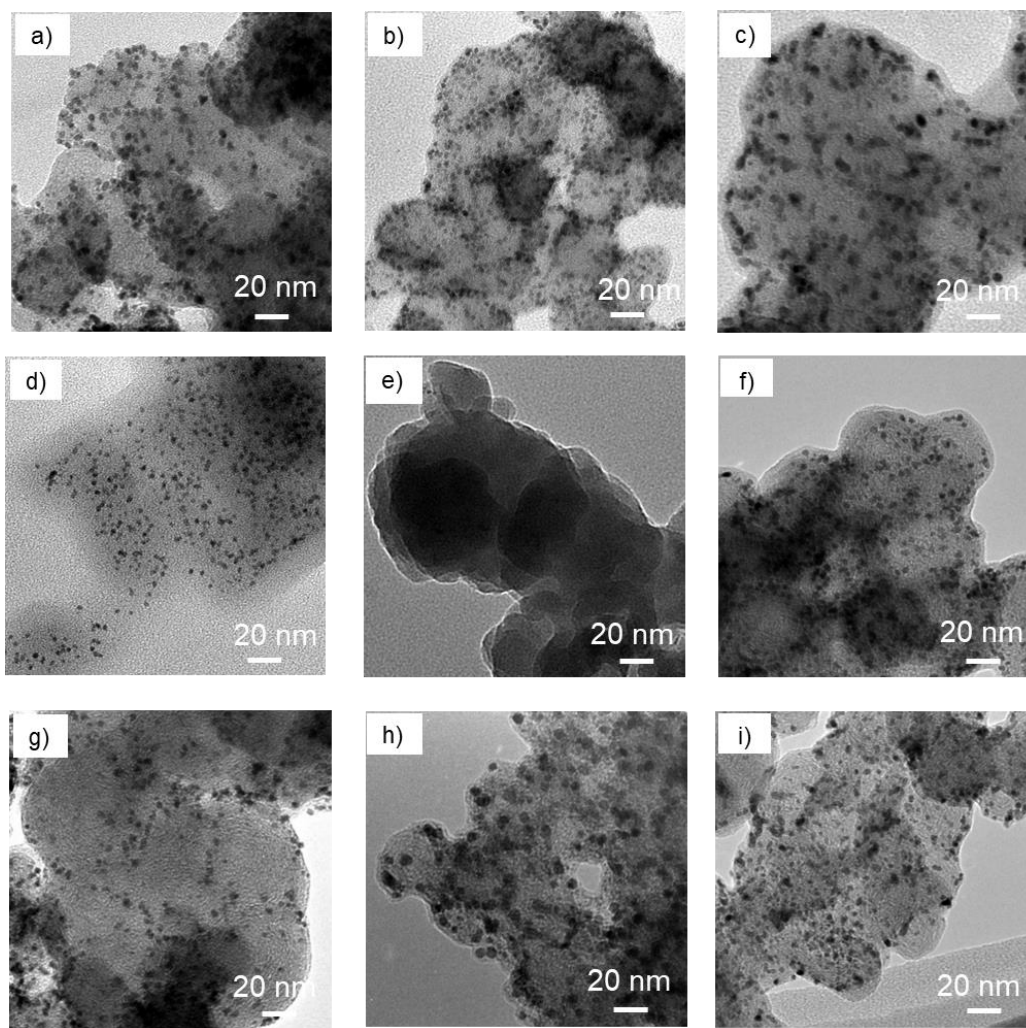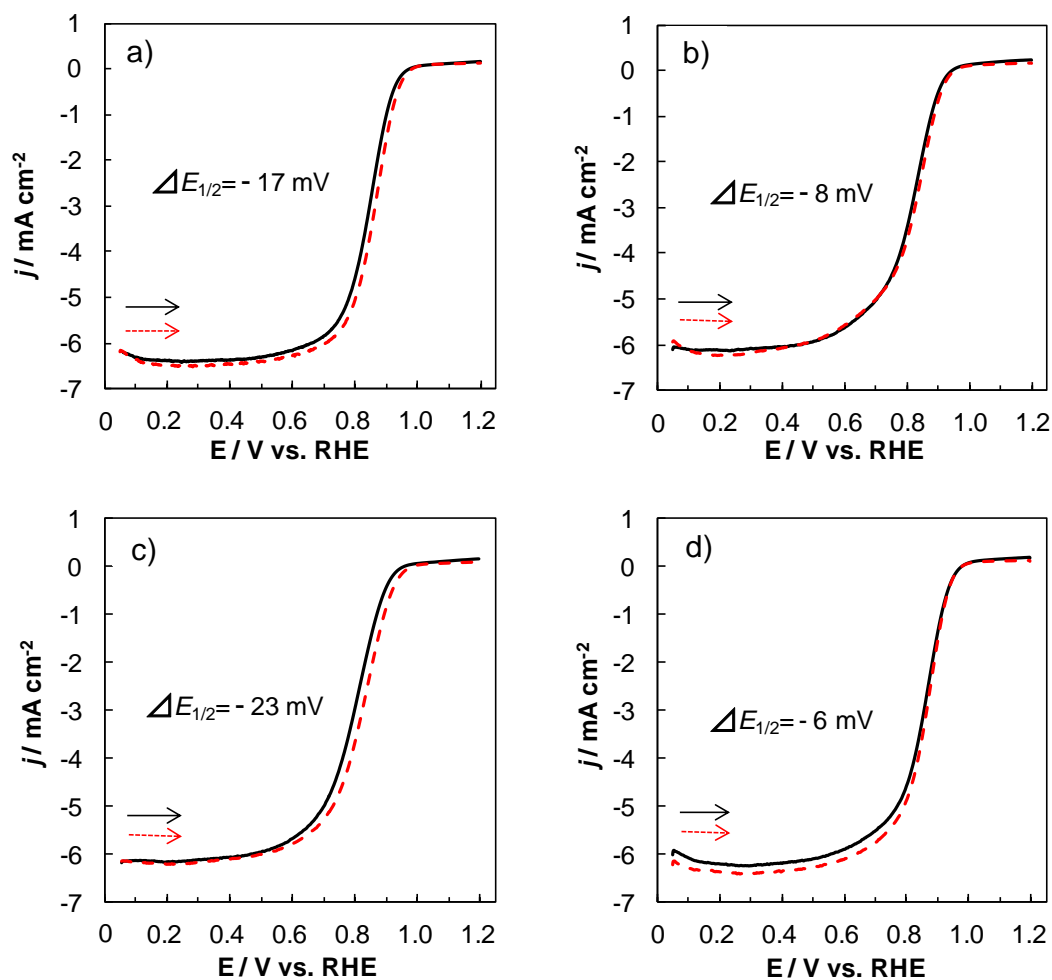
Fig. 4 TEM images of the Pt nanoparticle-supported carbon catalysts used in this research: (a) Pt/[PhNH$_3$][HSO$_4$]·**1**/C, (b) Pt/3MT·**1**/C, (c) Pt/diphenylamine·**2**/C, (d) Pt/pyrrole·**1**/C, (e) Pt/EDOT·**1**/C, (f) Pt/[DPA][HSO$_4$]·**1**/C, (g) Pt/–·**1**/C, (h) Pt/–·**2**/C and (i) TEC10V30E.
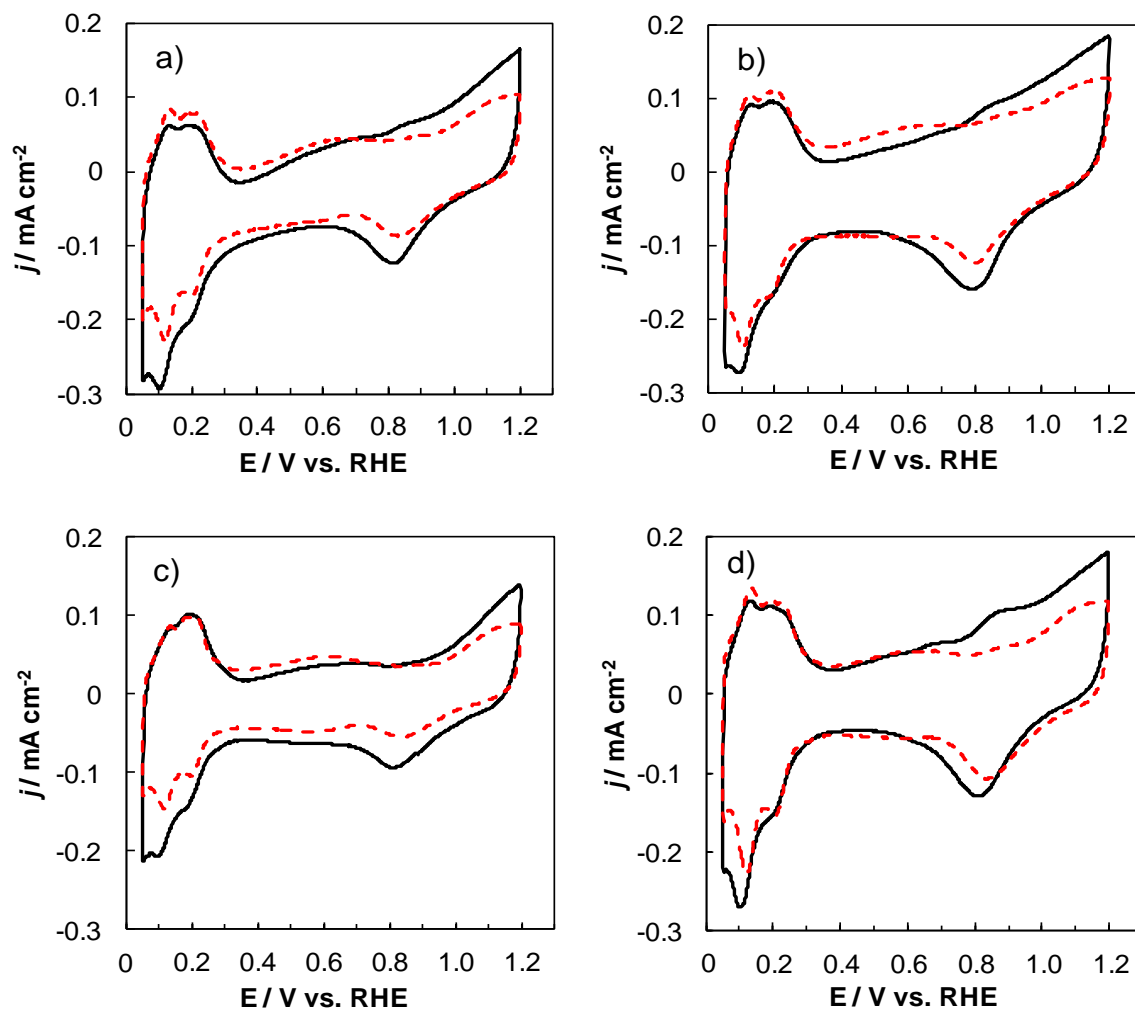
Fig. 5 Cyclic voltammograms recorded at the different catalysts in a N$_2$-saturated 0.1 M HClO$_4$ aqueous solution before (—) and after (- - -) the durability test. The catalysts were: (a) Pt/[PhNH$_3$][HSO$_4$]·**1**/C, (b) Pt/3MT·**1**/C, (c) Pt/diphenylamine·**2**/C and (d) Pt/[DPA][HSO$_4$]·**1**/C. The scan rate was 10 mV s^{-1}.
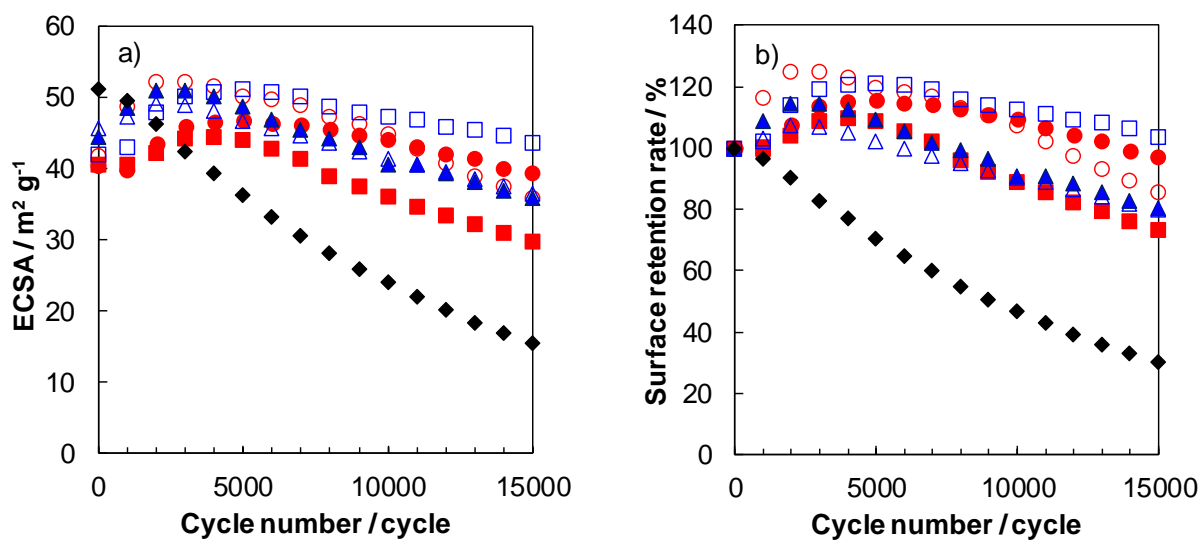
Fig. 6 Variation in the a) ECSA and b) surface retention rate for the ECSA estimated from Fig. 6a as a function of cycle number: ● Pt/[PhNH$_3$][HSO$_4$]·**1**/C, ○ Pt/3MT·**1**/C, ■ Pt/diphenylamine·**2**/C, □ Pt/[DPA][HSO$_4$]·**1**/C, ▲ Pt/−·**1**/C, △ Pt/−·**2**/C and ◆ TEC10V30E.

Fig. 7 Hydrodynamic voltammograms recorded in an O_2-saturated 0.1 M $HClO_4$ aqueous solution of (a) Pt/[PhNH$_3$][HSO$_4$]·**1**/C, (b) Pt/3MT·**1**/C, (c) Pt/diphenylamine·**2**/C and (d) Pt/[DPA][HSO$_4$]·**1**/C electrodes before (—) and after (- - -) durability test. The revolution speed was 1,600 rpm. The scan rate was 10 mV s^{-1}.
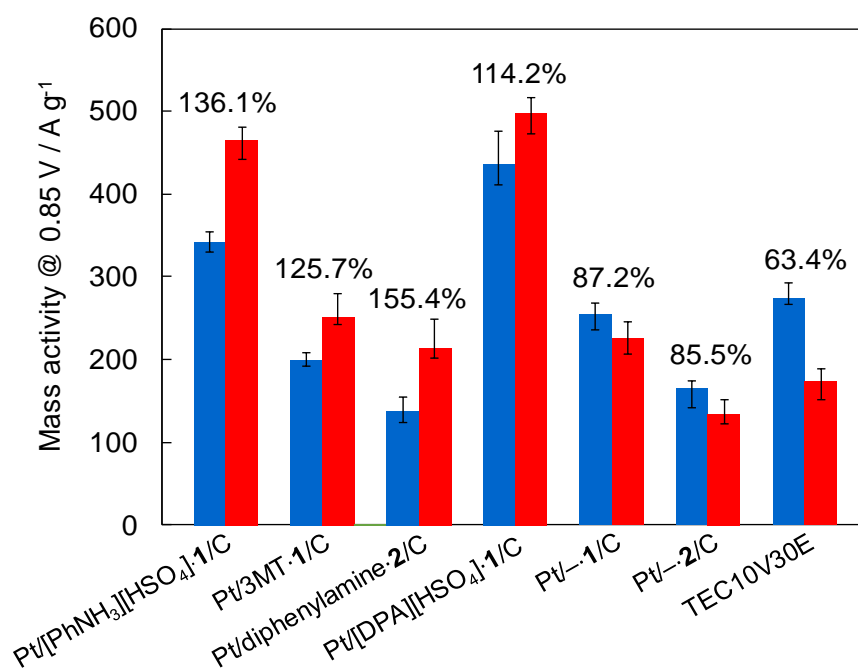
Fig. 8 Comparison of mass activities of the electrocatalysts before (blue) and after (red) the durability test (15,000 cycles).

Table 1 Summary of the Pt nanoparticle-supported carbon catalysts used in this research

Catalyst	Used Additives / ILs	Mean particle size (nm)	Pt loading amount (wt%)	ECSA			Mass activity			$\Delta E_{1/2}{}^b$ (mV)
				Initial ($m^2\,g^{-1}$)	After 15,000 cycles ($m^2\,g^{-1}$)	Retention rate^a (%)	Initial ($A\,g^{-1}$)	After 15,000 cycles ($A\,g^{-1}$)	Retention rate^a (%)	
Pt/[PhNH$_3$][HSO$_4$]· **1**/C^c	[PhNH$_3$][HSO$_4$] / [DEMA][HSO$_4$]	2.7 (0.6)^e	20.4	40.4	39.4	97.5	341.9	465.4	136.1	- 17
Pt/3MT· **1**/C^c	3MT / [DEMA][HSO$_4$]	2.6 (0.5)^e	21.1	41.9	36.0	86.0	199.4	250.6	125.7	- 8
Pt/diphenylamine· **2**/C^d	diphenylamine / [N$_{1,1,1,3}$][Tf$_2$N]	3.4 (1.0)^e	20.2	40.6	29.7	73.3	138.1	214.6	155.4	- 23
Pt/[DPA][HSO$_4$]· **1**/C^c	[DPA][HSO$_4$] / [DEMA][HSO$_4$]	2.9 (0.5)^e	23.0	42.1	43.6	103.5	436.1	498.1	114.2	- 6
Pt/–· **1**/C^c	— / [DEMA][HSO$_4$]	2.6 (1.1)^e	23.8	44.6	36.0	80.7	255.2	224.2	88.0	3
Pt/–· **2**/C^d	— / [N$_{1,1,1,3}$][Tf$_2$N]	3.6 (1.0)^e	23.2	45.8	36.6	79.9	165.2	134.9	81.6	1
TEC10V30E	– / –	2.6 (0.8)^e	26.2	51.3	15.5	30.2	273.7	173.6	63.4	41

^{a} After 15,000 cycles. ^{b} $\Delta E_{1/2}$ is the shift in the half wave potential between before and after durability test in Fig. 7 and Fig. S6†. ^{c} **1** indicates [DEMA][HSO$_4$]. ^{d} **2** indicates [N$_{1,1,1,3}$][Tf$_2$N]. ^{e} The values in parentheses are standard deviations.

Table of contents entry

We demonstrated that conductive polymer formation between Pt nanoparticles and carbon supports contributes to the catalytic performance for oxygen reduction.

Reiko Izumi, Yu Yao, Tetsuya Tsuda,* Tsukasa Torimoto and Susumu Kuwabata*

Oxygen reduction electrocatalysts sophisticated by using Pt nanoparticle-dispersed ionic liquids with electropolymerizable additives

ToC figure